Group Constants Generation and SPH Correction Applied to the Westinghouse LFR design

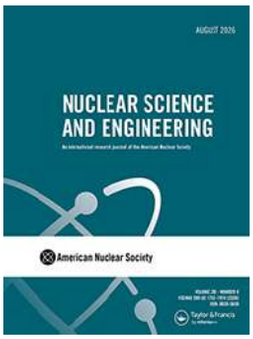

Nuclear Science and Engineering

ISSN: 0029-5639 (Print) 1943-748X (Online) Journal homepage: www.tandfonline.com/journals/unse20

Group Constants Generation and SPH Correction Applied to the Westinghouse LFR Design

Christian Vita , Nicolo' Abrate , Sandra Dulla & Fausto Franceschini

To cite this article: Christian Vita , Nicolo' Abrate , Sandra Dulla & Fausto Franceschini (22 May 2026): Group Constants Generation and SPH Correction Applied to the Westinghouse LFR Design, Nuclear Science and Engineering, DOI: 10.1080/00295639.2026.2667086

To link to this article: https://doi.org/10.1080/00295639.2026.2667086

Published online: 22 May 2026.

NUCLEAR SCIENCE AND ENGINEERING

DOI: https://doi.org/10.1080/00295639.2026.2667086

Group Constants Generation and SPH Correction Applied to the Westinghouse LFR Design

Christian Vita[a], Nicolo' Abrate[a], Sandra Dulla[a], and Fausto Franceschini[b]

[a]*NEMO Group, Energy Deepartment, Politecnico di Torino, Turin, Italy;* [b]*Nuclear Fuels, Westinghouse Mangiarotti SPA, Monfalcone, Italy*

Received July 30, 2025
Accepted for Publication April 17, 2026

Abstract — *This paper presents a neutronic analysis of a simplified version of the Westinghouse lead-cooled fast reactor. The study focuses on the approach for generating the multi-group constants, obtained from Monte Carlo simulations, which are then used in the full-core calculations with deterministic codes. Specifically, this work investigates the possibility of using a set of sub-assembly models instead of a full-core model for the group constant generation when multiple core configurations are considered, to exploit the resulting computational advantages. The potential of applying the superhomogenization (SPH) method, through which SPH correction factors are generated and used to improve the accuracy of results obtained by deterministic models, is also explored. The use of super-cell models for non-multiplying regions and theirs adoption for generating SPH correction factors to material data in regions that cause significant neutron flux gradients is also illustrated. The values of k_{eff} and the power density distribution show good agreement with the Monte Carlo reference results after cross-section correction, the kinetic parameter Λ_{eff} does not seem to be affected by SPH, and the β_{eff} is more sensitive to the correction, although this does not always lead to improved results.*

Keywords — *Lead cooled fast reactor, SPH, cross-section generation, Monte Carlo, neutronics, deterministic solver.*

I. INTRODUCTION

In recent years, interest in lead-cooled fast reactor (LFR) technology has grown, as it supports the development of nuclear plants that aim at producing clean, efficient, and safe energy. LFRs operate at higher temperatures than light water reactors and can run at low pressure due to the use of liquid lead as a coolant. Additionally, as fast-spectrum reactors, LFRs can more efficiently fission isotopes such as plutonium and minor actinides, thus helping reducing long-term nuclear waste. For these reasons, companies such as Westinghouse electric company (WEC) have started developing their own LFR designs.

Significant research efforts are directed toward gaining a deeper understanding and addressing various long-standing questions concerning LFRs. In the field of neutronics, the method for generating multi-group constants plays an important role. Thanks to increasing computational power, the adoption of Monte Carlo (MC) codes to collapse and homogenize nuclear data has gained more relevance, thanks to their ability to use continuous-energy and continuous-angle representations while modeling the system geometry in great detail. Multi-group nuclear data collapsed through an MC code can be generated using two main strategies: (1) using different assembly-level systems to try to represent the whole core in different conditions and (2) using a full-core model and defining different regions in which the user wants to homogenize and collapse the continuous nuclear data into multi-group nuclear data. In this study, both strategies are used and compared.

CONTACT Christian Vita christian.vita@polito.it

Multi-group data are typically generated for deterministic code-based simulations, which have the significant advantage of requiring relatively short computational time. However, deterministic codes often rely on assumptions and simplifications that may compromise result accuracy. Specifically, the deterministic model developed and used in this study is a diffusion solver that requires a set of multi-group data homogenized at the assembly level, a spatial discretization using the finite element method (FEM), and the implementation of the neutron diffusion equation. To improve the outputs of the deterministic solver, in this work we test the possibility of applying superhomogenization (SPH) correction factors [1] to the group constants of the material regions that cause the larger discrepancy in the power distribution of the LFR design. The application of the SPH method to liquid metal fast reactor designs has already been investigated in several studies [2–4]. These works served as references for the present study, whose main objective is to apply the SPH technique to the Westinghouse LFR design and to analyze the general trends of the results obtained using different multi-group cross-section (MGXS) generation strategies, both with and without the SPH method. Furthermore, this work aims to demonstrate the simplicity and nonintrusive nature of the SPH approach. The method can be implemented without major modifications to the structure of an existing neutronic code, requiring only a straightforward two-step workflow. This feature makes the SPH technique particularly suitable for integration into generic, homemade solvers. In this study, the multi-group data are generated by the MC code Serpent2 [5,6], while the deterministic solver adopted was developed in FreeFEM++ [7].

II. WESTINGHOUSE LFR SIMPLIFIED MODEL

The core model used in this study is a simplified representation of the Westinghouse LFR at the beginning of life (BOL), shown in Fig. 1. It consists of four radial enrichment regions—the inner core, middle core, external core, and outer core—with ^{235}U content increasing progressively from the center toward the outer region. The active core is surrounded by a layer of lead and the structural material of the vessel. In total, there are 18 control rods (CRs). At BOL, the fuel is axially homogeneous, and in this simplified model, no additional axial components (e.g., springs or insulators) are considered.

Two reactor configurations are analyzed: the all-rods-in (ARI) case and the all-rods-out (ARO) case. The reference results are generated using a full-core Serpent model with 50 inactive cycles, 1000 active cycles, and 10^6 particles per cycle. Vacuum boundary conditions are imposed on both the axial and radial boundaries. The reference k_{eff}, β_{eff}, Λ_{eff} values for each configuration are reported in Table 1, and the corresponding power density distributions are shown in Fig. 2.

It is important to highlight the high level of symmetry of the system, allowing us to simulate only 1/12 of the core.

In this study, a relatively small number of universes for multi-group data generation have been considered, for reasons such as reducing as much as possible the statistical error coming from MC simulations and also keeping the problem simple, easing the solution of the full-core deterministic model downstream the pipeline. Thus, the set of multi-group constants are generated for each FA type plus an additional one, confined in the very central region of the core, in order to capture the spectrum change due to the

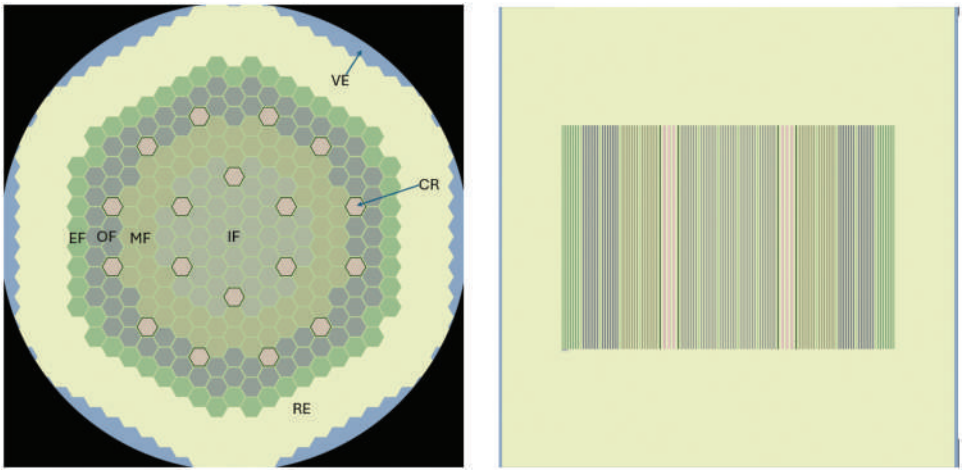

Fig. 1. Radial (left) and axial (right) views of the Serpent2 model of the LFR simplified core. The core is surrounded by the lead reflector (re) and by the vessel material (ve). The core has four different fuel assemblies (FAs) with a specific ^{235}U content: (from the lower-graded to the higher) inner fuel (IF), middle fuel (MF), outer fuel (OF), external fuel (EF).

TABLE 1

ARI and ARO Reference Results Computed with Serpent2.

	k_{eff} (-)	β_{eff} (pcm)	Λ_{eff} (μs)
ARI	$0.89763 \pm 4.4 \times 10^{-5}$	712.3 ± 1.4	$0.99253 \pm 2.08 \times 10^{-3}$
ARO	$1.06336 \pm 4.0 \times 10^{-5}$	696.1 ± 1.26	$0.89968 \pm 1.46 \times 10^{-3}$

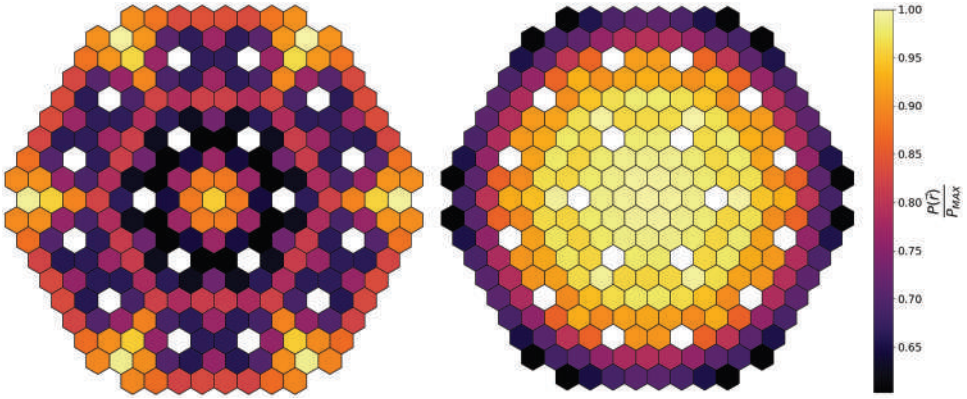

Fig. 2. Serpent power density distribution for ARI (left) and ARO (right) configuration.

presence of the first ring of CRs. In Fig. 3a, the spectrum change in the so-called central fuel can be observed, where with $\bar{\phi}_i$ and $\bar{\phi}_{tot}$, we refer to the neutron flux spectrum divided by the volume of the corresponding region "i" and the total neutron spectrum divided by the total volume of the core, respectively.

In the axial direction, two more regions are defined at the top and the bottom part of each FA to assess spectral changes along the axes, as seen in Fig. 3b, where the spectrum in different axial positions of different FAs is shown. For the following calculations, a five-group energy grid is adopted. The few-groups boundaries are (in MeV): 1×10^{-11}, 9.1188×10^{-3}, 6.7379×10^{-2}, 1.8316×10^{-1}, 1.3530, 20.0. The grid structure was selected based on the reference grid defined in Ref. [8] for the ALFRED design. The well-known ECCO-33 grid was reduced to a five-group energy grid by performing a spectrum analysis in the most relevant regions of the core. Using fewer energy groups helps decrease the computational time required by the deterministic solver and reduces the uncertainty associated with MGXS, particularly in the thermal energy region. In Fig. 3c, the total spectrum of the system with the energy grid boundaries is shown.

III. METHODOLOGY

To carry out this study, a Python package was implemented, with the main task of managing various data types and selecting the desired dataset for the deterministic solver. The workflow consists of first launching the Serpent2 simulations for both the full-core and the mini-core models to obtain multi-group data. Then, through an input file, it is possible to select a subset of regions belonging to the "non-multiplying regions" family and correct the data using SPH coefficients (described later). Once the data are prepared, the dataset can be selected with any desired option, whether SPH-corrected or not. Finally, the generated dataset is used as input for the deterministic solver developed in FreeFEM++. The obtained results are then compared with the reference values provided by the full-core MC simulations. The calculation of the kinetic parameters β_{eff}, Λ_{eff} is based on double-weighting formulations [9]; thus, the adjoint function is calculated as well.

It is worth mentioning here that there is a gap in the literature concerning the calculation of kinetic parameters when the SPH correction is applied. To the best of the authors' knowledge, the studies addressing this aspect only apply the "non-fundamental" SPH method, where the correction is made in systems with vacuum boundary conditions, which is not the case in this study, such as in Refs. [10–12].

III.A. Serpent Models for Multi-Group Nuclear Data Generation

Full-core MC simulations accurately capture spatial flux gradients in the group constant generation process.

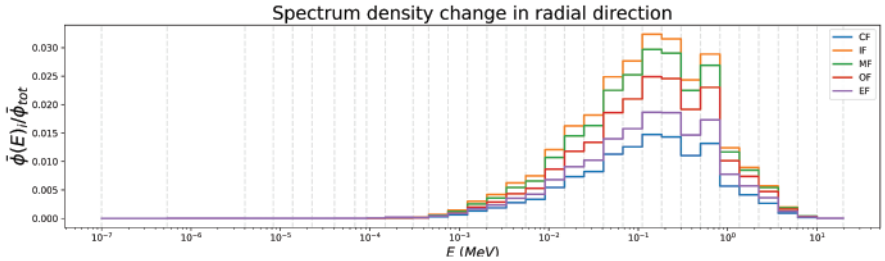

(a) Reactor spectrum change in the radial direction. For this representation the ECCO33 energy grid is used. The maximum Serpent2 relative uncertainty is in the most thermal energy group of the CF region and it is equal to 13%.

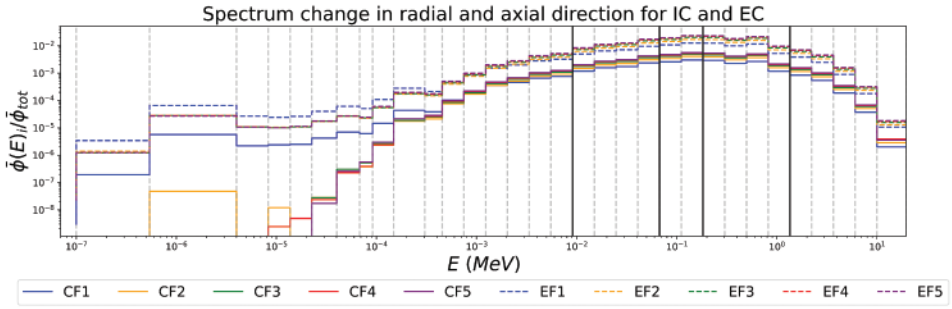

(b) Reactor spectrum change in Central Fuel (CF), and External Fuel (EF) for five axial cuts, from the top (labeled with number 1) of the core to its center (labeled with number 5). For this representation the ECCO33 energy grid is used. The maximum Serpent2 relative uncertainty is in the most thermal energy group of the CF5 region and it is equal to 15%.

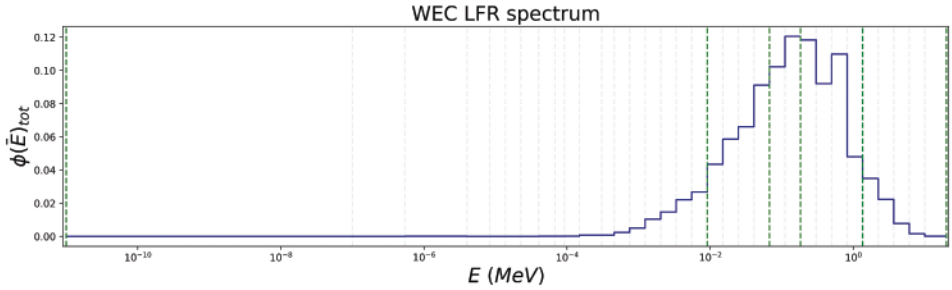

(c) Total system spectrum. The dashed green lines represent the selected few-groups grid cuts used in this study. The maximum Serpent2 relative uncertainty is in the most thermal energy group and it is equal to 8%.

Fig. 3. Analysis of the energy spectrum in different regions in the LFR core and definition of the five-group structure adopted.

However, they face challenges in estimating data with sufficient statistics for regions far from the core and are computationally intensive, particularly when the evaluation of multiple core configurations is required for transient analyses. For these reasons, the default approach is still to use a set of assembly-level systems, also called in this work "mini-core." The mini-core modes used in this study can be divided into three families:

1. *Model for non-peripheral FA* Used to model the FAs located in the inner rings of the core. The model consists of a single 3D fuel with reflective boundary conditions in the radial direction and vacuum boundary conditions in the axial direction (see Fig. 4a).

2. *Model for non-multiplying assembly*: 2D model where the non-multiplying element (CR/SR, upper/lower reflector, coolant, shielding) is defined in the center, surrounded by FAs. Reflective boundary conditions are applied radially (see Fig. 4b). Since in the full-core model, the CRs face two different types of FAs, two different approaches are used: The first is easier to implement and considers a single-type FA surrounding the CR, generally the most numerous in the actual pattern. The second option tested in this work is to reproduce the exact pattern of the FAs surrounding the CR. Although a 3D model with vacuum boundary conditions in the axial direction could be employed, this work adopts a 2D model. Previous studies have shown that accurate results can be

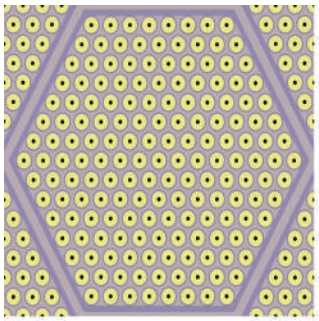

(a) Radial view of the 3D mini-core model for non-peripheral fuel assembly.

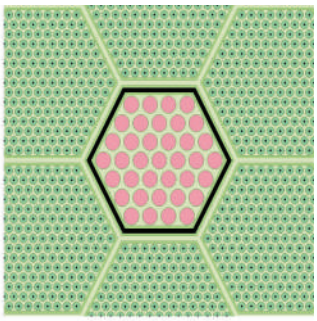

(b) View of the 2D mini-core model for non multiplying assembly.

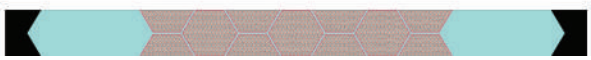

(c) Radial view of the 3D mini-core model for peripheral fuel assembly.

Fig. 4. Serpent mini-core models.

achieved even when axial effects are neglected, particularly for test cases in which all CRs are either fully inserted or fully withdrawn, as in the present study [3].

3. *Model for peripheral FA*: Used to model the FAs located in the external ring of the core. It is a 3D mini-core model composed of only the FAs of the peripheral multiplying assemblies surrounded by the radial reflector (coolant) and by the shielding. This system has vacuum boundary conditions both radially and axially (see Fig. 4c).

It is important to take care of the specific design characteristics and, if necessary, tailor the systems under analysis to the specific design needs. For the Westinghouse LFR system, the mini-core models defined are as follows:

1. One mini-core of type "non-peripheral fuel" for the four FA regions: CF, IF, MF, and OF (see Fig. 4a).

2. One mini-core model for all the non-multiplying material regions present in the system, which are the first ring of the CR, the second ring of the CR—both rodded and unrodded—shield, the radial reflector, and the axial reflector (see Fig. 4b).

3. One mini-core of type "peripheral fuel" for the more external ring of FAs, labeled as EF (see Fig. 4c).

Thus, a total of 12 Serpent models need to be simulated. Regarding the computational time, with the same number of active/inactive cycles used in the full-core case and particles per cycle, mini-core systems require less running time, though the difference is not always significant. Naturally, the overall time required for the mini-core option is greater, but if more than one core configuration is considered (i.e., changing the CR positions or the fuel arrangement), a new MC full-core simulation must be performed for each configuration. Therefore, full-core simulations quickly become inefficient in terms of computational time required (as mentioned in Ref. [13]). On the other hand, in principle, each time a distributed variable (e.g., the temperature or the depletion stage of the system) needs all the minicore models to be launched again to obtain the new multi-group data that account for the new distributions.

III.B. SPH Algorithm for the Deterministic Solver

The main goal of the SPH method is to preserve the reaction rates in selected regions of the system used to generate the SPH coffiecients. For this purpose, a supercell model is reproduced in the deterministic code as in the full-core simulation, homogenizing the regions and solving the eigenvalue problem iteratively using the corrected data until the difference between the new SPH coefficients and the previous ones is below a fixed tolerance. The SPH equations are:

$$\begin{aligned}\tau^{\mathrm{ref}}_{x,r,g} &= \tau^{\mathrm{FF}}_{x,r,g} = \Sigma^{*}_{x,r,g}\phi^{\mathrm{FF}}_{r,g} = \mu_{r,g}\Sigma^{\mathrm{ref}}_{x,r,g}\phi^{\mathrm{FF}}_{r,g} \\ &= N_g \frac{\phi^{\mathrm{ref}}_{r,g}}{\phi^{\mathrm{FF}}_{r,g}}\Sigma^{\mathrm{ref}}_{x,r,g}\phi^{\mathrm{FF}}_{r,g} = \frac{\sum_r V_r \phi^{\mathrm{FF}}_{r,g}}{\sum_r V_r \phi^{\mathrm{ref}}_{r,g}} \frac{\phi^{\mathrm{ref}}_{r,g}}{\phi^{\mathrm{FF}}_{r,g}}\Sigma^{\mathrm{ref}}_{x,r,g}\phi^{\mathrm{FF}}_{r,g}\,, \end{aligned} \tag{1}$$

where τ refers to reaction rates, $\Sigma_{x,r,g}$ to a generic cross-section for region r and group g, $\phi_{r,g}$ to the neutron flux

in group g and region r, V_r to the region volume/area, and $\mu_{r,g}$ to the correction factor. The SPH method is formulated as a fixed-source problem, and due to the absence of constraints on the SPH factors, it admits an infinite number of possible solutions. To ensure a unique set of SPH factors, a normalization condition must be applied: In the original SPH approach, this is achieved by enforcing the preservation of the flux averaged over the entire geometry of the supercell through the equivalence procedure. The normalization factor, N_g, is defined as the ratio of the sum of the spectrum in each region [14]. The superscripts "ref" and "FF" refer to the Serpent reference results and the homogenized FreeFEM++ model results, respectively. The tuned multi-group data are $\Sigma_{t,g}$, D_g, $\Sigma_{g'\to g}$, $\nu\Sigma_{f,g}$. Concerning the scattering matrix, the production scattering matrix has been considered in this study. If (n, xn) was neglected, there would be a systematic understimation of neutron production, leading to a smaller reactivity. As proposed in Ref. [3], only non-multiplying regions, such as the CRs and the empty CR channels, are subjected to the SPH procedure described in Fig. 5. In Fig. 6, an example of an SPH coefficient and a mini-core k_{eff} convergence example is shown.

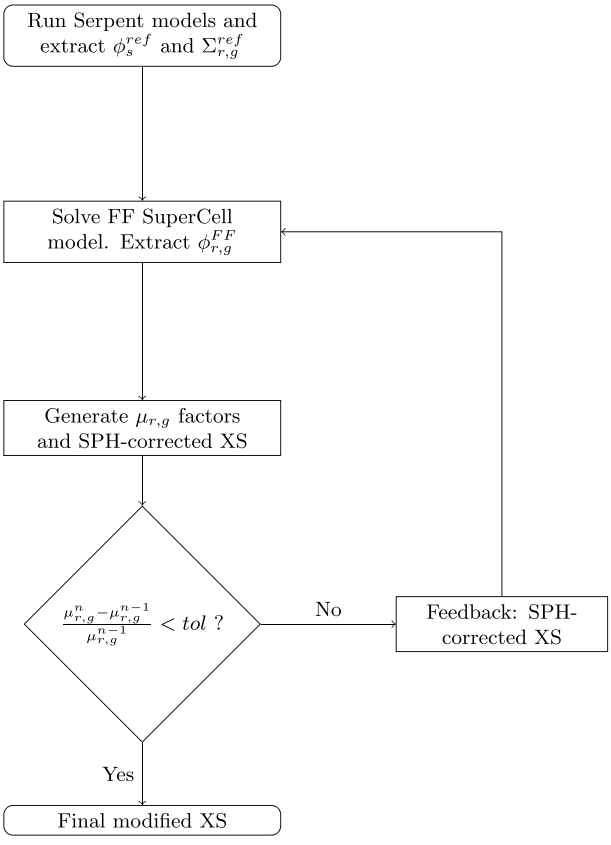

Fig. 5. SPH algorithm flowchart.

Thus, the non-multiplying mini-core is defined in FreeFem++ by homogenizing the assemblies. The eigenvalue problem of the neutron diffusion equation is then solved until the difference between the SPH coefficients reaches a fixed tolerance value. Fig. 6 shows an example the evolution of the relative errors of the total reaction rates of the different reaction channels both for the inactive and fuel regions of the defined supercell with the CR inserted as central assembly. Along the single total reaction rate evolution, the k_{eff} evolution over the iterations of the mini-core model is reported.

In Table 2, the SPH factors are reported for the inner and outer regions of the CR assembly in both configurations—with and without CR insertion—and for each assembly type present in the models. The central region of the supercell is denoted as $r = 1$, corresponding to the CR in the inserted configuration and to the lead region in the extracted configuration, while all surrounding FAs constitute region $r = 2$. The most significant corrections occur in the central region of the inserted configurations, indicating that the deterministic model lacks accuracy in predicting the neutron flux in this area. This limitation may be critical when the solver is used without an MC reference, for example, in transient analyses.

III.C. Full-Core FreeFEM++ Solver

In this work, a deterministic 3D neutron diffusion solver developed in FreeFEM++ is used to assess the influence of using MGXS generated from both full-core and mini-core models. The FEM solver was chosen because the neutronic tool developed in this work is intended to be applicable not only to the LFR design considered here but also to highly compact microreactor concepts currently under development at Westinghouse, such as eVinci. These systems feature complex geometries and unconventional core layouts, where FEM offers greater flexibility and accuracy compared to traditional nodal methods. These models are considered in two configurations: with and without SPH corrections. The analysis follows an assembly-wise homogenization approach, where each FA is treated as a homogenized region to simplify the modeling while preserving accuracy at the core level. Due to the high degree of radial symmetry in the reactor core, along with some geometric simplifications in the axial direction, where non-active materials are removed, only half of the axial geometry is represented in the model. As a result, the total geometry modeled is reduced by a factor of 24 compared to the full physical system. In Fig. 7, the

TABLE 2

SPH Factors for All Corrected Regions.

			$\mu_{r,g=1}$	$\mu_{r,g=2}$	$\mu_{r,g=3}$	$\mu_{r,g=4}$	$\mu_{r,g=5}$
Inner CR model	Inserted	$r=1$	0.84647	0.90426	0.89596	0.84977	0.74205
		$r=2$	1.03507	1.02211	1.02123	1.02392	1.02686
	Extracted	$r=1$	0.9224	0.99970	0.99801	1.00384	1.02469
		$r=2$	1.02199	1.00009	1.00065	0.99867	0.99077
Outer CR model	Inserted	$r=1$	0.84648	0.90396	0.89546	0.84945	0.74123
		$r=2$	1.0350	1.02214	1.02128	1.02385	1.02675
	Extracted	$r=1$	0.92253	0.99953	0.99771	1.00349	1.02334
		$r=2$	1.02196	1.00015	1.00075	0.99879	0.99132

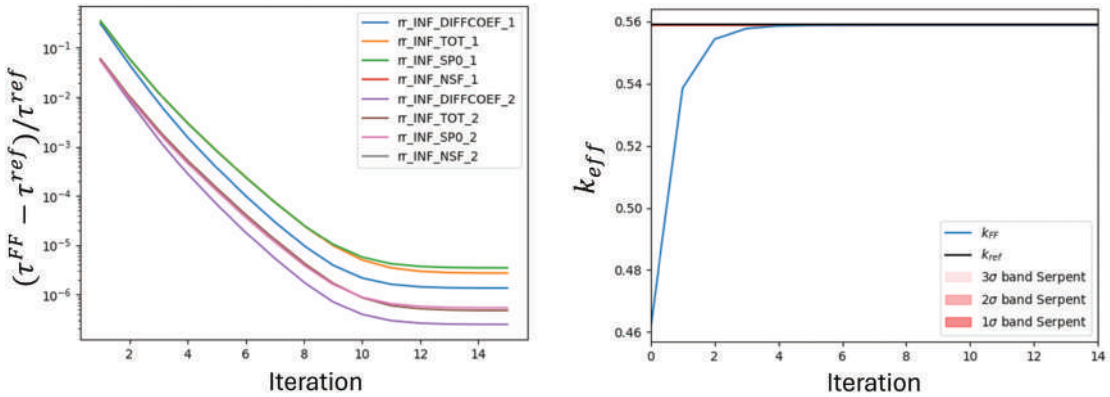

Fig. 6. SPH method convergence example. Left panel: Relative differences in reaction rates (names consistent with the Serpent2 output) between the FreeFEM++ model and the reference Serpent2 results for the different multi-groups constants (MGC) evolutions of the two mini-core assemblies: central cr material (subscript "1") and surrounding FA (subscript "2"). Right panel: Evolution of k_{eff} over the iterations of the equivalent FreeFEM++ model.

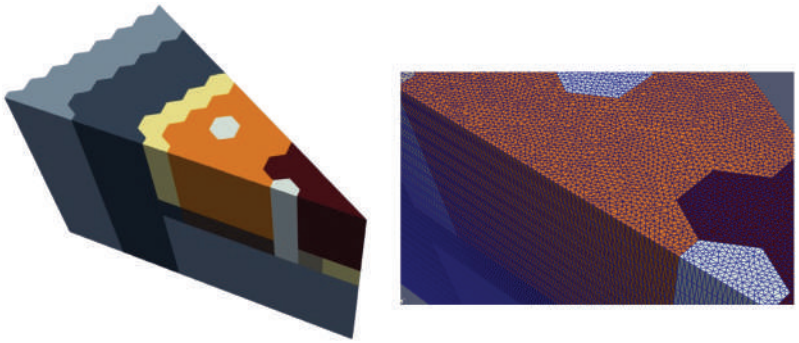

Fig. 7. WEC LFR full-core model in FreeFEM++ (left) and the adopted mesh for every full-core symulation (right).

geometry model is shown together with the mesh used for each full-core calculation. The mesh was generated using the open-source software Gmsh [15], employing prismatic elements. It is important to note that no dedicated mesh optimization study was performed, as this lies beyond the scope of the present work. Nevertheless, grid independence was verified by adopting a sufficiently fine mesh, made feasible by the relatively low computational cost of the deterministic model.

One important feature of FreeFEM++ is that it requires the user to explicitly define the weak formulation of the governing equations. Accordingly, the neutron diffusion equation must be reformulated in its variational form to be implemented and solved within the FreeFEM++ environment. The resulting formulation is:

$$\int_{\Omega} \nabla\left(D_g(\vec{r})\,\phi_g(\vec{r})\,w_g\right) d\vec{r} + \int_{\Omega} \Sigma_{t,g}(\vec{r})\,\phi_g(\vec{r})\,w_g\,d\vec{r} = \frac{1}{k_{\text{eff}}} \int_{\Omega} \chi_g(\vec{r})\,w_g \sum_{g'=1}^{G} \nu\Sigma_{f,g'}(\vec{r})\,\phi_{g'}(\vec{r})\,d\vec{r} + \int_{\Omega} w_g \sum_{g'=1}^{G} \Sigma_{g'\to g}(\vec{r})\,\phi_{g'}(\vec{r})\,d\vec{r} + \int_{\Omega} \nabla(w_g \nabla\phi_g) d\vec{r} \tag{2}$$

where w_g are the test functions for each energy groups and the last term on the right-hand side, based on the Gauss–Green theory, can be rewritten as:

$$\int_{\Omega} \nabla(w_g \nabla\phi_g) d\vec{r} = \int_{\partial\Omega_v} w_g \nabla\phi_g \cdot \hat{n} dS \tag{3}$$

At this point, the P_1 angle treatment model is used for the outgoing current definition in presence of vacuum boundaries, turning Eq. (3) into:

$$\int_{\partial\Omega_v} w_g \nabla\phi_g \cdot \hat{n} dS = -\int_{\partial\Omega_v} \frac{1}{2} w_g \phi_g dS \tag{4}$$

Thus, the neutron diffusion equation is solved for each energy group, using a different dataset each time, combining SPH-corrected and uncorrected MGXS data in different assembly type of the core.

The kinetic parameters calculated, namely the effective delayed neutron fraction, β_{eff}, and the effective prompt neutron generation time, Λ_{eff} are:

$$\beta_{eff} = \frac{\langle \phi^{\dagger} | \hat{F}_d \phi \rangle}{\langle \phi^{\dagger} | \hat{F}_t \phi \rangle} \tag{5}$$

$$\Lambda_{eff} = \frac{\left\langle \phi^{\dagger} \middle| \frac{1}{v} \phi \right\rangle}{\langle \phi^{\dagger} | \hat{F}_t \phi \rangle} \ . \tag{6}$$

To obtain the adjoint flux $\phi^{\dagger}$, necessary for their evaluation, the neutronic problem must be solved twice. The second solution involves computing the adjoint function by transposing the operators on the right-hand side of the neutron diffusion equation without modifying the structure of the left-hand side. For the adjoint solution of the problem, the non-corrected MGXS are used, since previous studies [10] have shown that applying the SPH method is not always advantageous when addressing the adjoint problem. Specifically, the results show that restricting SPH to the fuel region in the forward flux calculation enhances the preservation of kinetics parameters. Conversely, extending SPH to the adjoint calculation for the k-eigenvalue introduces inconsistencies in the bilinear weighting of these parameters, thereby reducing the reliability of the results. Therefore, for the adjoint problem, SPH should generally be avoided or applied with great caution, as it may compromise the accuracy of the kinetics parameter preservation.

IV. RESULTS

In this section, the results obtained from the FreeFEM++ 3D full-core model are analyzed. Several datasets are considered and compared with each other and with the Serpent2 reference results. The analyzed outputs include k_{eff}, Λ_{eff}, β_{eff}, and the fission power density distribution. The datasets used for the ARI and ARO configuration simulations are described in Table 3.

TABLE 3

Datasets Used for Results Comparison Description.

Dataset name	Dataset description
full-core	All regions data from Serpent MC full-core model.
full-core + CR SPH	All regions data from MC full-core model. CR data are corrected.
mini-core	All regions data from MC mini-core models.
mini-core + CR SPH	All regions data from MC mini-core models. CR data are corrected.
mini-core w CR detailed	All regions data from MC mini-core models. Improved CR Serpent model.
mini-core w CR detailed + CR, SFA SPH	All regions data from MC mini-core models. Improved CR Serpent model. CR and surrounding FAs (SFAs) are corrected.

TABLE 4

Comparison of Different Core Models and MGC Generation Methods.

	Full-core	Full-core + CR SPH	Mini-core	Mini-core + CR SPH	Mini-core + CR detailed	Mini-core + CR detailed + CR and SFA SPH
Δk_{eff} (pcm)						
ARI	−1023	−101	−1068	−65	−961.5	−18.9
ARO	152	43	−23	13	22	11
$RMSE_P$ (%)						
ARI	8.3	2.3	8.8	2.4	7.4	1.3
ARO	0.28	0.23	0.42	0.26	0.30	0.21
$Max(E_p)$ (%)						
ARI	11.66	2.38	10.64	3.92	8.6	3.97
ARO	1.54	1.64	1.75	2.61	2.1	1.39
$\Delta\beta_{eff}$ (pcm)						
ARI	31	39	43	41	43	33
ARO	−35	−34	−30	−29	−34	−36
$\Delta\Lambda_{eff}$ (%)						
ARI	−2	−1.8	1.6	−1.9	2	−2
ARO	−17	−17	−17	−17	−32	−32
$t_{dataset}$ (h)						
ARI	12.3	24.5	70.2	70.2	70.2	70.2
ARO	14.1	34.4	78.6	78.6	78.6	78.6

All results of this study are summarized in Table 4; however, the discussion will first focus on k_{eff} and the assembly-wise relative error of the fission power density. Figs. 9 and 10 show the corresponding results for the ARI configuration.

It can be observed that the SPH correction improves the results for both k_{eff} and the fission power density distribution. Specifically, the difference in the eigenvalue with respect to the reference Serpent2 value is −1023 pcm when the full-core dataset without SPH correction is used. By using the same dataset but replacing the CR MGC with the mini-core data and applying the SPH factors, the difference is reduced to −101 pcm. Regarding the relative error of the fission power density, the root mean square error (RMSE) decreases from 8.3% for the first dataset to 2.3% for the second. When the dataset composed only of MGCs generated from the mini-core models is used, the results are basically comparable with those obtained using the full-core dataset. This suggests that the mini-core models accurately represent the system neutron spectrum. The best results are obtained when using the last dataset of Table 3, with an

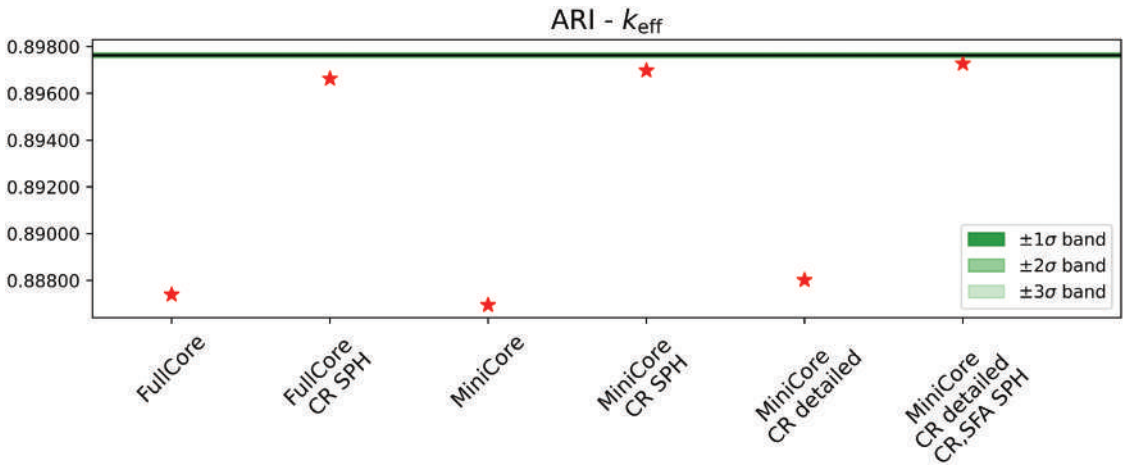

Fig. 8. ARI configuration k_{eff}. The green bands represent the statistical error of the reference results.

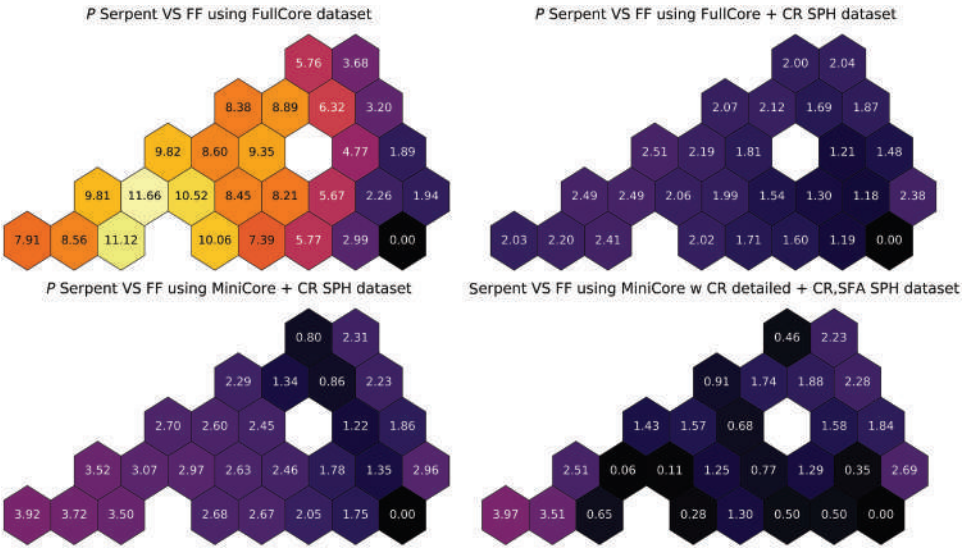

Fig. 9. Absolute total 3D power density relative error between ff simulations and Serpent reference results $\left(\left|\frac{P_{\text{ref}}-P_{\text{FF}}}{P_{\text{ref}}}\right| \%\right)$ of each assembly of the ARI configuration.

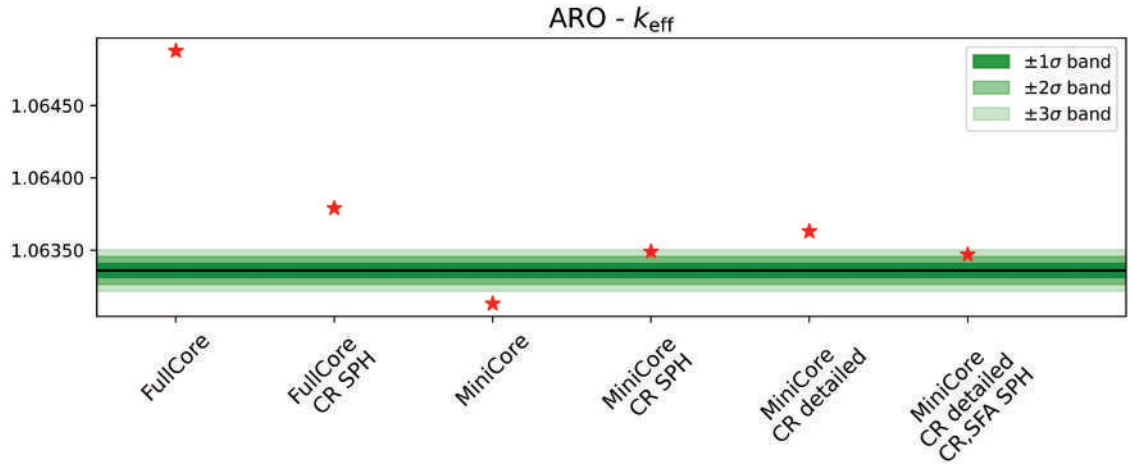

Fig. 10. ARO configuration k_{eff}. The green bands represent the statistical error of the reference results.

eigenvalue difference of 19 pcm and a power RMSE of 1.3%.

Figs. 8 and 9 show the corresponding results for the ARO configuration.

In the ARO configuration all the CRs are extracted; thus, the heterogeneity in the power distribution is less significant than in the ARI case. Therefore, the accuracy gained once the SPH factors are used is comparable with the cases in which uncorrected datasets are used. The deterministic solver provides a k_{eff} and power RMSE equal to 152 pcm and 0.25%, respectively, when the full-core dataset is used. By using the same dataset but replacing the CR MGC with the mini-core data and applying the SPH factors, the difference is reduced to 43 pcm for the eigenvalue and 0.23% for the power RMSE. It is worth noting that even if the mini-core dataset provides good agreement with the multiplication eigenvalue, it also gives a relatively bad prediction for the distributed considered quantity, with the highest RMSE equal to 0.42. In general, k_{eff} value can hide more easly error compensation than distributed quantity such as power density.

For both configurations, the k_{eff} obtained using the full-core dataset yields the least accurate result. On the contrary, all cases that utilize the detailed CR description model and apply corrections to CR and SFA data produce the most accurate results. It is important to recall that the SPH method enforces the reaction rates in the

SPH-corrected regions to match those of the reference mini-core model. If this reference model properly represents the flux distribution in the corresponding region of the full-core calculation, the corrected solution will naturally provide very similar results. However, it is clear that the deterministic model without SPH correction shows noticeable deviations, which are likely due to the limited number of energy groups and/or the limited number of universes defined in Serpent2 for MGXS generation. These limitations can affect the accuracy of the uncorrected solution. Nevertheless, it is important to emphasize that all comparisons were performed under consistent modeling conditions, which makes the observations drawn from the current results still meaningful and valid within the scope of this study. Finally, one of the most interesting advantages of the SPH method is precisely its ability to mitigate the dependency of deterministic results on the chosen energy group structure or the spatial subdivision used for collapsing nuclear data. This feature makes SPH particularly attractive for practical applications where computational efficiency and accuracy must be balanced.

In Fig. 12, the kinetic parameters results of both core configurations are reported and compared with the Serpent reference values.

The kinetic parameters, β_{eff} and Λ_{eff}, as expected, do not receive any beneficial from the SPH correction method: In contrast to reaction rates, which are preserved via SPH equivalence theory, there is no guarantee that the kinetic parameters obtained from Serpent are likewise preserved in the deterministic code calculations. In other words, applying a bilinear weighting that uses the forward and adjoint multigroup flux computed by the deterministic code to collapse the kinetic parameters β_{eff}, Λ_{eff} does not necessarily ensure the preservation of the reference values derived from Serpent. If the reaction rates are preserved, it is not possible to preserve at the the bilinear reaction rate. While SPH equivalence theory offers a method to preserve reaction rates by modifying cross-sections, there remains a theoretical gap regarding the homogenization of bilinear quantities, such as kinetic parameters, in particular if SPH correction is applied only to some sub-regions of the core, as was the case in this study.

It would not be entirely accurate to claim that the two kinetic parameters are insensitive to the applied corrections. As shown in Fig. 11, variations in the parameters are observed when different datasets are employed. In particular, for β_{eff}, only minor changes are noted across the different datasets. This behavior can be better understood by considering the definition provided in Eq. (5), where the numerator includes the delayed fission operator $\hat{F}_d$, defined as $\beta\chi_d\nu\Sigma_f$. This term vanishes in non-fissile regions, such as CR assemblies. Therefore, the limited impact of dataset variation on β_{eff} is expected. Nonetheless, the small differences that do appear can be attributed to secondary effects. Specifically, the SPH correction modifies the cross-sections in the CR regions, which in turn alters the local neutron flux near the CR assemblies. These flux perturbations, though subtle, cause the slight deviations observed in the calculated values of β_{eff}.

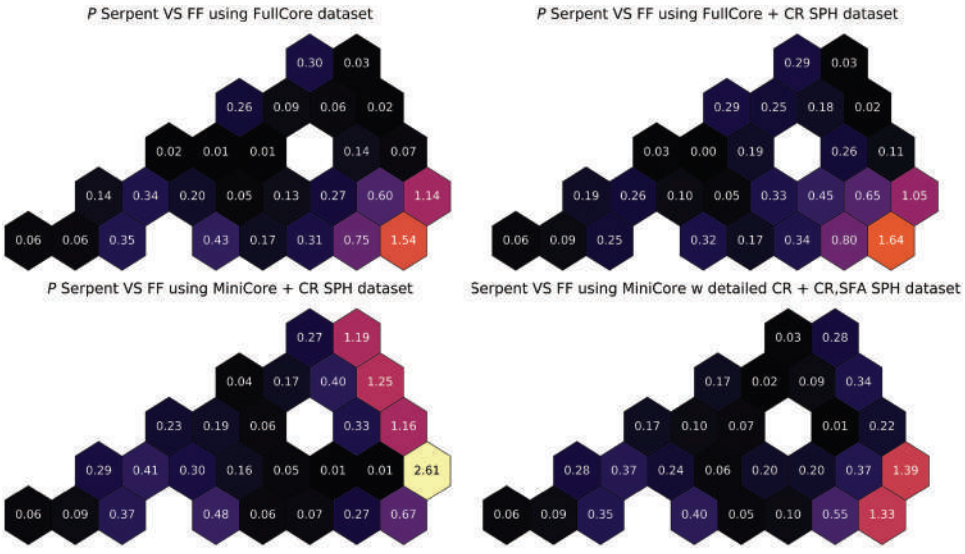

Fig. 11. Absolute total 3D power density relative error between ff simulations and Serpent reference results $\left(\left|\frac{P_{\text{ref}}-P_{\text{FF}}}{P_{\text{ref}}}\right|\%\right)$ of each assembly of the ARO configuration.

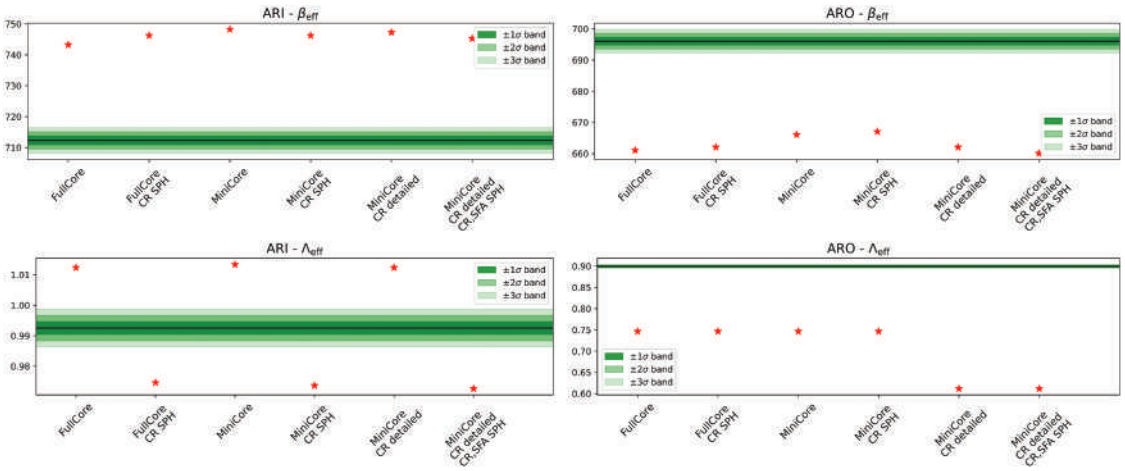

Fig. 12. ARI (left) and ARO (right) configuration β_{eff} and Λ_{eff} comparison. The green bands represent the statistical error of the reference results.

Regarding the behavior of Λ_{eff} in the ARI test case, it can be observed that the kinetic parameter is consistently underestimated when SPH corrections are applied and overestimated when no correction is used. As shown in Eq. (6), the numerator of the expression is non-zero since the term $\frac{1}{v}$ is always finite. The variation in the numerator arises from changes in the neutron flux ϕ, which is influenced by the application of SPH factors. On the other hand, the denominator remains unchanged because the corrections affect only the CR regions, where the fission cross-section Σ_f is zero; hence, no contribution is introduced in those areas. In contrast, for the ARO configuration, Λ_{eff} remains nearly constant across the first few datasets. This is because the only varying component in the expression for Λ_{eff} is the neutron flux, which does not significantly change in the ARO case, as also evident in Fig. 12. However, when the last two datasets are considered, a noticeable reduction in Λ_{eff} is observed. This can likely be attributed to the fact that, in these datasets, the SPH correction is extended not only to the CR assemblies but also to the surrounding FAs. Consequently, the denominator of the expression for Λ_{eff} changes (in this specific case, it increases), due to the inclusion of non-zero fission terms, leading to a variation (decrease) of the overall value of the kinetic parameter.

All the previously discussed results are summarized in Table 4, along with additional information, such as the maximum power density relative error (E_p) and the computational time required to generate the multi-group data. It can be observed that the computational time for building the dataset when mini-core models are employed is higher. One of the advantages of adopting mini-core models lies in avoiding full MC simulations each time the core configuration changes—such as in the case of CR repositioning or fuel reshuffling—since these models are defined independently from the surrounding assembly pattern (except for the non-multiplying mini-core model type). However, the use of mini-core models can become less practical when multiple parameters, such as temperatures, must be considered, as this would require regenerating the dataset for each parameter.

Based on the configurations tested, the most efficient case in terms of computational time is the "full-core" model. The second most efficient is the "full-core + CR SPH" dataset, since it requires only a full-core simulation plus two mini-core models for the CR MGC. All remaining cases rely on mini-core models, which require approximately 70 h of MC calculations to generate the complete dataset. These calculations were performed on a PC equipped with an Intel Xeon Gold 6130 CPU at 2.1 GHz, utilizing 30 cores.

As previously discussed, the "mini-core + CR detailed + CR and SFA SPH" configuration provides the most accurate results for both core configurations. Nevertheless, when balancing accuracy and computational cost, the "full-core + CR SPH" option emerges as the most favorable overall.

V. CONCLUSIONS

This paper investigates the possibility of reproducing Serpent2 reference results for the Westinghouse LFR core design using an FEM-based code to solve the neutron diffusion equation. To achieve this, various approaches for generating multi-group constants were explored, including the use of a standard full-core model and a set of mini-core models representative of the different regions within the system. The advantage of using mini-core models has been

highlighted in terms of not only result accuracy but also computational time. Using mini-core modeling can be advantageous when multiple core configurations (e.g., CR positions) need to be analyzed. In contrast, full-core models can require a significant amount of computational time, especially if a low statistical error is desired in non-multiplying regions or for materials located far from the core (e.g., shielding). On the other hand, this advantage does not necessarily hold when multi-group data libraries must be generated for several parameters, such as temperatures and burnup levels. In such cases, relying on mini-core models can quickly become inefficient, as the full set of simulations (which in this study required approximately 70 h for all mini-core models using the same neutron population settings values in Serpent2) would need to be repeated for every temperature ($N_{\text{temperature}}$) and burnup step (N_{burnup}). This results in a total computational effort scaling with $N_{\text{temperature}} \times N_{\text{burnup}}$, making the approach potentially impractical for large parametric studies unless a highly reliable deterministic code is employed for data generation. Such a code should be capable of accurately reproducing the neutron spectrum within the system and of extracting the information required to compute the SPH correction coefficients. It is important to note, however, that using the same number of particles and active and inactive cycles for both full-core and mini-core models was a deliberate choice to simplify the comparison of results. Mini-core models generally require fewer histories, particularly for cells with reflective boundary conditions. In fact, by adopting a more tailored number of cycles for each model—while preserving comparable cross-section accuracy—the total computational time can be reduced significantly, down to approximately 48 h for the ARI configuration and 53 h for the ARO configuration. This observation has been added here to provide a clearer perspective on the potential for optimization.

Furthermore, the study demonstrates how to apply the SPH method to tune multi-group data with the aim of improving reference quantities. The integral values k_{eff}, β_{eff}, Λ_{eff} and the power density distribution were selected for results comparison. The time required for the SPH-correction algorithm has not been reported, as it is negligible (of the order of seconds for each supercell analyzed).

The power density distribution and k_{eff} generally show good agreement with the deterministic model when the SPH method is applied. In the ARO configuration, the simulation based on the mini-core model dataset is less sensitive to the SPH correction due to the lower heterogeneity of the system. Overall, the models relying on the full-core dataset produce poorer results. It is important to mention here that the SPH method proves particularly effective in fast reactor applications due to the relatively uniform neutron flux, reduced anisotropy, and smoother energy-dependent cross-sections, which minimize multigroup collapsing errors and allow scalar correction factors to preserve global kinetics parameters with high fidelity.

The values of β_{eff} and Λ_{eff} were obtained using the double-weighting formulation. The results indicate that the kinetic parameters are sensitive to the cross-section correction, but this does not lead to any direct improvement since the SPH method is meant to preserve the reaction rates given by the multiplication of a macroscopic cross-section and the neutron flux, $\Sigma_x\phi$, not with the adjoint function.

Looking ahead, this work will continue to build on the advantages of using mini-core modeling for multi-group data generation, particularly in uncertainty and sensitivity analysis related to nuclear data for transient analysis. Future efforts will also aim to improve the accuracy of kinetic parameter reproduction when applying SPH correction.

Author Contributions

CRediT: **Christian Vita:** Conceptualization, Formal analysis, Investigation, Methodology, Software, Visualization, Writing – original draft, Writing – review & editing; **Nicolo' Abrate:** Supervision, Writing – review & editing; **Sandra Dulla:** Funding acquisition, Project administration, Supervision, Writing – review & editing; **Fausto Franceschini:** Project administration, Supervision, Writing – review & editing.

Disclosure Statement

No potential conflict of interest was reported by the author(s).

Funding

This work was supported by the "Piano Nazionale di Ripresa e Resilienza" (PNRR) and Westinghouse Electric Company, which co-funded the first author's PhD research activity (PhD contract DM 117). Computational resources were provided by HPC@PoliTO and CLOUD@PoliTo, a project of Academic Computing within the Department of Control and Computer Engineering at Politecnico di Torino.

References

1. A. Hébert, "Développement de la Méthode SPH: Homogénéisation de Cellules dans un Réseau Non Uniforme et Calcul des Parametres de Réflecteur," PhD Thesis, CEA Centre d'Etudes Nucleaires de Saclay, Service d'Etudes de Criticite (1980).

2. C. Luo et al., "Application of Full-Core Three-Dimensional Multi-Physics Calculation to the EBR-II SHRT-45R Benchmark," *Ann. Nucl. Energy*, **208**, 110786 (2024); https://doi.org/10.1016/j.anucene.2024.110786.

3. E. Nikitin, E. Fridman, and K. Mikityuk, "On the Use of the SPH Method in Nodal Diffusion Analyses of SFR Cores," *Ann. Nucl. Energy*, **85**, 544 (2015); https://doi.org/10.1016/j.anucene.2015.06.007.

4. R. Rachamin and S. Kliem, "Validation of the DYN3D-Serpent Code System for SFR Cores Using Selected BFS Experiments. Part II: DYN3D Calculations," *Ann. Nucl. Energy*, **114**, 181 (2018); https://doi.org/10.1016/j.anucene.2017.12.036.

5. J. Leppänen et al., "The Serpent Monte Carlo Code: Status, Development and Applications in 2013," *Ann. Nucl. Energy*, **82**, 142 (2015); https://doi.org/10.1016/j.anucene.2014.08.024.

6. J. Leppänen, M. Pusa, and E. Fridman, "Overview of Methodology for Spatial Homogenization in the Serpent 2 Monte Carlo Code," *Ann. Nucl. Energy*, **96**, 126 (2016); https://doi.org/10.1016/j.anucene.2016.06.007.

7. F. Hecht, "New Development in FreeFEM++," *J. Numer. Math.*, **20**, *3–4*, 251 (2012); https://doi.org/10.1515/jnum-2012-0013.

8. V. Fabrizio et al., "ALFRED Reactor: Evaluation of Multi Temperature Cross Section Sets by Deterministic and Stochastic Methods," ENEA (2013).

9. G. Bell and S. Glasstone, *Nuclear Reactor Theory*, Van Nostrand Reinhold Company, New York (1970).

10. C. Takasugi et al., "Preservation of Kinetics Parameters Generated by Monte Carlo Calculations in Two-Step Deterministic Calculations," *EPJ Nucl. Sci. Technol.*, **9**, INL/JOU-21–65377–Rev000 (2023); https://doi.org/10.1051/epjn/2022056.

11. C. M. Mueller, C.-S. Lin, and J. Ortensi, "NRC Multiphysics Analysis Capability Deployment FY 2021-Part 2," (2021); https://doi.org/10.2172/1812179.

12. J. Ortensi et al., "Validation of the Griffin Application for TREAT Transient Modeling and Simulation," *Nucl. Eng. Des.*, **385**, 111478 (2021); https://doi.org/10.1016/j.nucengdes.2021.111478.

13. Y. Wu et al., "Development and Verification of a Monte Carlo Two-Step Method for Lead-Based Fast Reactor Neutronics Analysis," *Nucl. Eng. Technol.*, **55**, *6*, 2112 (2023); https://doi.org/10.1016/j.net.2023.03.006.

14. J. Ortensi et al., "A Newton Solution for the Superhomogenization Method: The PJFNK-SPH," *Ann. Nucl. Energy*, **111**, 579 (2018); https://doi.org/10.1016/j.anucene.2017.09.027.

15. C. Geuzaine and J.-F. Remacle, "Gmsh: A 3-D Finite Element Mesh Generator with Built-In Pre-and Post-Processing Facilities," *Int. J. Numer. Methods Eng.*, **79**, *11*, 1309 (2009).